Self-Assembled Structures of Giant Surfactants Exhibit a Remarkable Sensitivity on Chemical Compositions and Topologies for Tailoring Sub-10 nm Nanostructures
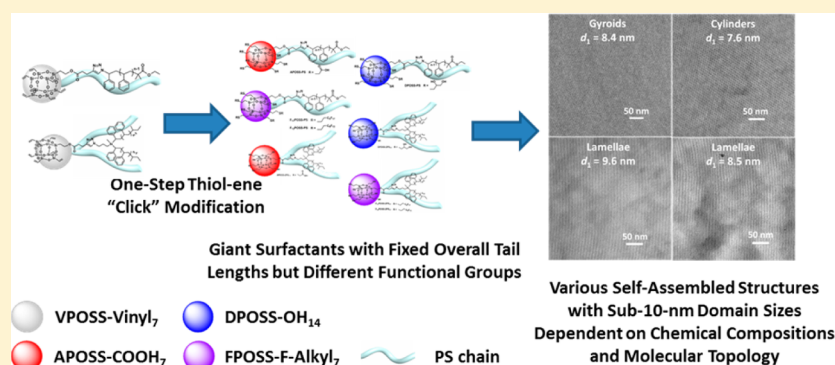
Kan Yue,[†] Chang Liu,[†] Mingjun Huang,[†] Jiahao Huang,[†] Zhe Zhou,[†] Kan Wu,[†] Hao Liu,[†] Zhiwei Lin,[†] An-Chang Shi,*,[§] Wen-Bin Zhang,*,[‡] and Stephen Z. D. Cheng*,[†][iD]

[†]Department of Polymer Science, The University of Akron, Akron, Ohio 44325-3909, United States
[‡]Key Laboratory of Polymer Chemistry & Physics of Ministry of Education, Center for Soft Matter Science and Engineering, College of Chemistry and Molecular Engineering, Peking University, Beijing 100871, P. R. China
[§]Department of Physics and Astronomy, McMaster University, Hamilton, Ontario, Canada L8S 4M1

Ⓢ *Supporting Information*

Giant Surfactants with Fixed Overall Tail Lengths but Different Functional Groups

○ VPOSS-Vinyl$_7$ ● DPOSS-OH$_{14}$ ● APOSS-COOH$_7$ ● FPOSS-F-Alkyl$_7$ 〜 PS chain

Various Self-Assembled Structures with Sub-10-nm Domain Sizes Dependent on Chemical Compositions and Molecular Topology

ABSTRACT: We report a remarkable sensitivity of self-assembled structures of giant surfactants on their chemical compositions and molecular topology, which facilitate the engineering of various nanophase-separated structures with sub-10 nm feature sizes. Two classes of giant surfactants composed of various functionalized polyhedral oligomeric silsesquioxane (POSS) heads tethered with one or two polystyrene (PS) tails were efficiently prepared from common precursors of vinyl-substituted POSS−PS conjugates via one-step "thiol−ene" postpolymerization functionalization. With identical molecular weights of the PS tails, the resulting giant surfactants exhibited distinct highly ordered phases, as evidenced by small-angle X-ray scattering and transmission electron microscopy observations. Moreover, comparison between the topological isomers revealed that the self-assembled structures are also highly sensitive to molecular topology. Introduction of two PS tails with half-length not only shifted the boundaries between different ordered phases but also altered the packing configurations of the functional POSS cages, leading to further reduced feature sizes of the self-assembled nanodomains. Interestingly, a lower order−disorder transition temperature was also observed in the fluorinated F$_{13}$POSS tethered with two PS$_{17}$ tails, compared to its topological isomer composed of F$_{13}$POSS tethered with one PS$_{35}$ tail, indicating that the topological effect also existed in phase transition behaviors. These results provide insights to rationally design and precisely tailor self-assembled structures by controlling both primary chemical compositions and molecular topology in POSS-based giant surfactants.

INTRODUCTION

In recent years, research on self-assembling materials[1,2] and the resulting ordered structures[3−6] has been one of the central themes in the fields of polymers and materials science. In particular, the formation of self-assembled structures at sub-100 nm scale[7] has been extensively explored to develop alternative "bottom-up" nanopatterning and nanofabricating technologies to complement the conventional "top-down" lithographical methods.[8−14] Block copolymers are among the popular classes of self-assembling materials.[15−17] Formation of various self-assembled ordered structures, such as lamellae (Lam), hexagonally packed cylinders (Hex), body-centered cubic spheres (BCC), and bicontinuous double gyroid (DG) phases,[18] has been successfully achieved based on block copolymers via nanophase separation of the chemically incompatible blocks. In diblock copolymers, the phase behavior depends, *inter alia*, on the interaction parameter and degree of polymerization (χN) as well as the volume fraction (f).[15,18] Although ordered structures with characteristic dimensions of 5−100 nm have been widely reported in many diblock copolymer systems, creating self-assembled nanostructures at

Scheme 1. Syntheses of XPOSS-PS$_{35}$ and XPOSS-2PS$_{17}$ Giant Surfactants via the Thiol−Ene "Click" Reaction[a]
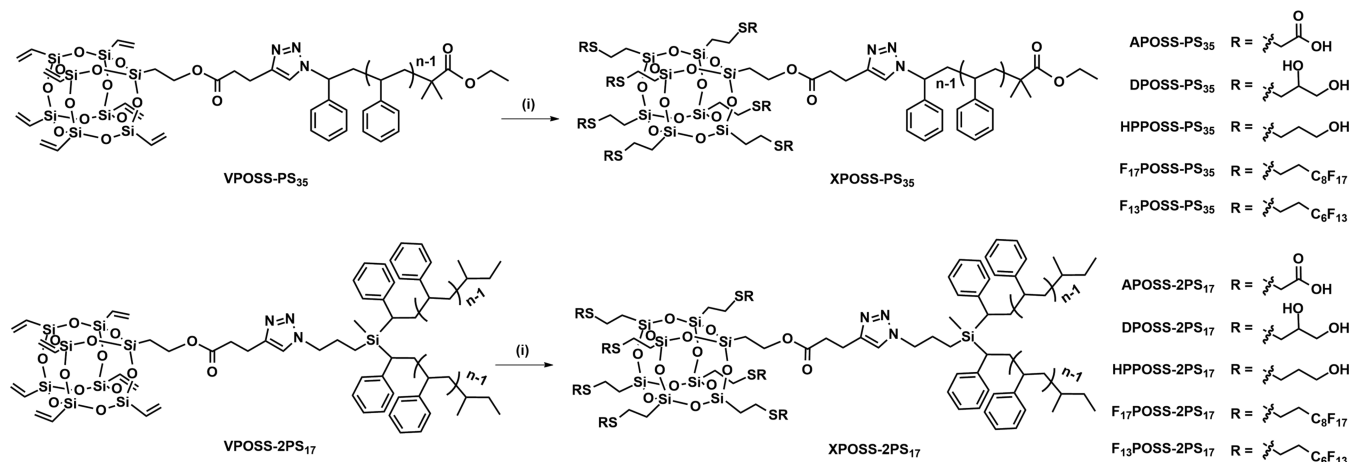
[a]Reactants and conditions: (i) thiol ligand R−SH, Irgacure 2959, THF, *hν*, 15−30 min, 66−85%.

sub-20 nm scale requires development of block copolymers that possess high χ values.[19] Recent examples of "high-χ" block copolymers include (1) a series of silicone-containing block polymers, such as poly(styrene-*b*-dimethylsiloxane) (PS-*b*-PDMS),[20−23] poly(2-vinylpyridine-*b*-dimethylsiloxane) (P2VP-*b*-PDMS),[24] poly(styrene-*b*-trimethylsilylstyrene-*b*-styrene) (PS-*b*-PTMSS-*b*-PS),[25] and poly(dimethylsiloxane-*b*-methyl methacrylate) (PDMS-*b*-PMMA),[26] (2) polylactide (PLA)-based block copolymers, such as poly(styrene-*b*-lactide) (PS-*b*-PLA),[27] poly(lactide-*b*-dimethylsiloxane-*b*-lactide) (PLA-*b*-PDMS-*b*-PLA),[28] poly(cyclohexylethylene-*b*-lactide) (PCHE−PLA),[29] and poly(4-trimethylsilylstyrene-*b*-lactide) (PTMSS-*b*-PLA),[25,30] (3) oligosaccharides-based block copolymers,[31−35] (4) block copolymers grafted with polyhedral oligomeric silsesquioxanes (POSS) as side chains,[36−41] (5) some other examples, such as poly(4-*tert*-butylstyrene-*b*-methyl methacrylate) (PtBS-*b*-PMMA),[42] poly(cyclohexylethylene)-*b*-poly(methyl methacrylate) (PCHE−PMMA),[43] and poly(4-*tert*-butylstyrene-*b*-2-vinylpyridine) (PtBuSt-*b*-P2VP),[44] among others.[45,46]

On the other hand, theoretical studies on the phase behaviors of AB$_n$ miktoarm star copolymers[47,48] predicted asymmetric phase diagrams and emphasized the role of AB interfaces in determining the phase-separated structures.[49−51] So far, researches on self-assembly of high-χ copolymers with diverse molecular topology are relatively limited.[41,52−54] Recently, Borsali, Satoh, and Kakuchi et al. reported the syntheses of several oligosaccharide-containing block copolymers with different molecular architectures and their self-assembly behaviors.[32,33,35] However, due to the rare availability of well-defined oligosaccharides as the building blocks, the structural variations of the oligosaccharide block are relatively restricted.

Our group has been devoted to the design and synthesis of a library of new self-assembling materials termed as "giant surfactants", which are based on polymer-tethered molecular nanoparticles (MNPs).[55−59] Examples are derivatives based on POSS[60−63] and [60]fullerene.[64−67] Facilitated by the high efficiency and modularity of the sequential "click" synthesis,[68−71] chemical structures of these giant surfactants can be systematically tuned by changing composition[68,72] and architecture[69] of the head and tail building blocks. Our POSS-based giant surfactants are different from the POSS-containing block copolymers reported by Hayakawa and Gopalan et

al.[36−41] because we use a single functionalized POSS cage as the replacement of a polymeric block, instead of grafting multiple POSS cages as the pedant groups. Our molecular design also allows changing the periphery functional groups on the POSS cage to tune interactions with the polymer tails.[68] Giant surfactants with various molecular architectures that resemble small-molecule surfactants,[73] lipids,[70] gemini surfactants,[69,74] and multiple-headed and multiple-tailed surfactants[69,75] have been successfully synthesized in high efficiency and structural precision,[68] providing a rich library of samples for exploring the structure−property relationships.

It has been observed that giant surfactants can self-assemble into various ordered structures in the bulk and thin film states.[75−79] For example, giant surfactants composed of one dihydroxyl-group-functionalized POSS cage and one PS tail (DPOSS-PS$_n$) can form a series of ordered phases, from Lam to DG and Hex and finally to BCC phase, by increasing the length of the PS tails. Because of the nanometer sizes of the POSS heads as one individual block, giant surfactants offer the opportunity to decrease the phase-separated domain size to below 10 nm.[75]

Herein, we report two series of POSS-based giant surfactants tethered with one or two PS tails as the model system to study how the self-assembled structures are influenced by both the chemical compositions and the molecular topology. Starting from two precursors of vinyl-substituted POSS−PS conjugates (VPOSS-PS$_{35}$ and VPOSS-2PS$_{17}$)[68,70] with statistically identical molecular weights and a rational selection of variously functionalized small molecule thiols, two series of giant surfactants with different functionalized POSS (XPOSS) heads can be prepared via a simple one-step thiol−ene reaction.[80−83] This platform ensures facile tuning of the volume fractions of the heads/tails, the packing and interactions among the heads, and the effective interaction parameter χ, thus allowing comparison between topological isomers of XPOSS-PS$_{35}$ and XPOSS-2PS$_{17}$ molecules with the same POSS functional groups. It is demonstrated that the resulting giant surfactants show distinct phases (e.g., Lam, DG, Hex, etc.) with feature sizes smaller than 10 nm, with a striking sensitivity to both chemical compositions and molecular topology.

Table 1. Summarized Characterization Data of XPOSS-PS$_{35}$ and XPOSS-2PS$_{17}$ Samples

sample	$M_{n,XPOSS}$[a] (kg/mol)	$M_{n,XPOSS-PS}$[a] (kg/mol)	$Đ$[b]	f_{PS}[c]	phase structure[d]	q_1[d] (nm^{-1})	d_1[d] (nm)
DPOSS-PS$_{35}$	1.5	5.2	1.04	0.78	DG	0.750	8.4
APOSS-PS$_{35}$	1.4	5.1	1.05	0.79	Hex	0.831	7.6
F$_{17}$POSS-PS$_{35}$	4.1	7.8	1.04	0.63	Lam	0.651	9.6
F$_{13}$POSS-PS$_{35}$	3.3	7.0	1.05	0.68	Lam	0.735	8.5
HPPOSS-PS$_{35}$	1.4	5.1	1.05	0.79	disordered		
DPOSS-2PS$_{17}$	1.5	5.2	1.03	0.78	Hex	0.912	6.9
APOSS-2PS$_{17}$	1.4	5.1	1.04	0.79	Hex	1.001	6.3
F$_{17}$POSS-2PS$_{17}$	4.1	7.8	1.03	0.63	Lam	0.787	8.0
F$_{13}$POSS-2PS$_{17}$	3.3	7.0	1.03	0.68	Lam	0.829	7.6
HPPOSS-2PS$_{17}$	1.4	5.1	1.04	0.79	disordered		

[a]These data are calculated based on NMR results. [b]These values are obtained from SEC data. [c]These values are calculated from $M_{n,NMR}$ and density values as elaborated in the Supporting Information. [d]These data are determined from SAXS patterns collected at room temperature.
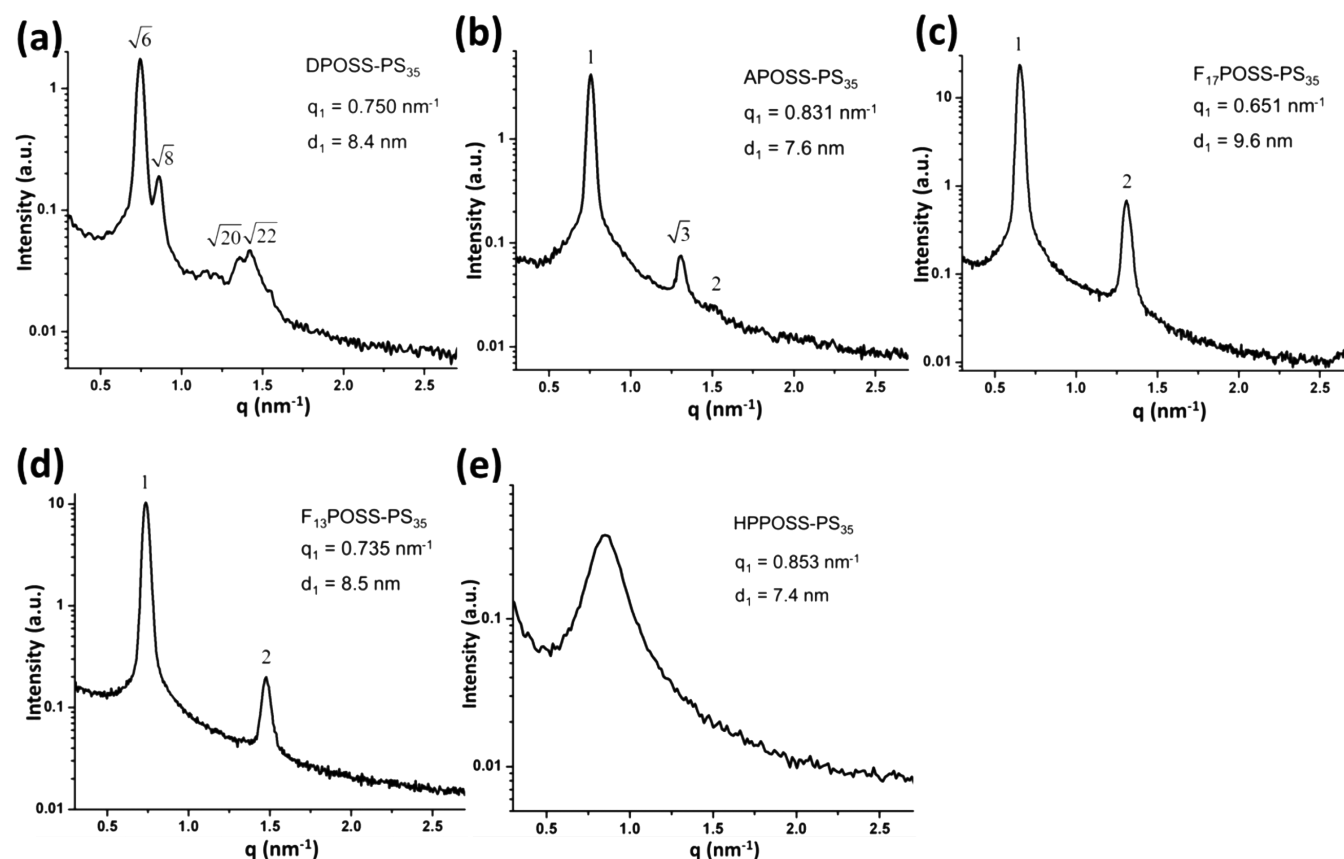

Figure 1. 1D SAXS patterns of (a) DPOSS-PS$_{35}$, (b) APOSS-PS$_{35}$, (c) F$_{17}$POSS-PS$_{35}$, (d) F$_{13}$POSS-PS$_{35}$, and (e) HPPOSS-PS$_{35}$. By fixing the length of the PS tails but changing the functional groups on the POSS cages, different phase structures are obtained.

■ RESULTS AND DISCUSSION

Design and Syntheses of Model Giant Surfactants. Our group has recently explored the methodologies to prepare POSS-based giant surfactants with diverse molecular architectures via the "sequential click" strategy.[68−70] Alkyne-functionalized vinyl-substituted POSS precursors were first "clicked" with azido-bearing polymers to afford VPOSS−polymer conjugates. In the following step, seven thiol ligands can be quantitatively introduced to the seven corners of the POSS cage via the photoinitiated "thiol−ene" reaction.[68] Seeking for a model system to study effects of POSS compositions and molecular topology on self-assembled nanostructures, we select two reported conjugates, VPOSS-PS$_{35}$ and VPOSS-2PS$_{17}$, as the precursors. Note that the overall molecular weights of the

PS chains are statistically the same for these two samples. Therefore, when functionalizing with the same thiols, the resulting XPOSS-PS$_{35}$ and XPOSS-2PS$_{17}$ giant surfactants can be viewed as pairs of topological isomers, which facilitates the isolation of the molecular architecture effect.

Syntheses of the two series of giant surfactants are outlined in Scheme 1. Before the thiol−ene modification, vinyl-substituted POSS cages cannot phase-separate with the PS tails (data not shown). As a result, to introduce chemical incompatibility between the XPOSS cages and PS tails, the selected thiol ligands have either polar groups such as carboxylic acid groups and hydroxyl groups[68] or perfluorinated alkyl chains.[72] The resulting functionalized POSS cages are denoted as APOSS for possessing seven carboxylic acid groups, DPOSS for having 14

hydroxyl groups, HPPOSS for possessing seven hydroxypropyl groups, F_{17}POSS for tethering seven $-C_8F_{17}$ fluorinated alkyl chains, and F_{13}POSS for having seven $-C_6F_{13}$ alkyl chains (Scheme 1).

According to our previous results, complete conversion of the vinyl groups and the precise chemical structures of the final products are confirmed by various molecular characterization techniques, such as ^{1}H NMR (Figures S1 and S2 in the Supporting Information), Fourier transform infrared spectroscopy (FT-IR) (Figures S3 and S4), and size exclusion chromatography (SEC) (Figures S5 and S6).[68−70] Detailed synthetic procedures can also be found in the Supporting Information. Because seven thiol molecules are simultaneously installed onto one POSS cage via the thiol−ene "click" reaction, even the seemingly slight molecular weight differences among the thiol ligands will result in non-negligible size differences of the XPOSS heads. The immediate consequence is that the volume fractions of the XPOSS heads and the PS tails depend on the selection of the thiol ligands (see Table 1 and Supporting Information for details). Furthermore, the effective interaction parameter χ between the XPOSS heads and the tails are also determined by the functional groups of the thiol ligands. These factors, together with the molecular topology, synergistically determine the nanophase separation behaviors of the XPOSS-PS$_{35}$ and XPOSS-2PS$_{17}$ giant surfactants.

After purifying the products, their thermal properties are examined by thermogravimetric analysis (TGA) and differential scanning calorimetry (DSC) techniques. From the TGA analysis, it is clear that these giant surfactants showed no obvious mass loss up to at least 210 °C under nitrogen (Figures S7 and S8). Their DSC data only showed one glass transition temperature of the PS tails (Figures S9 and S10). The as-synthesized samples were thermally annealed at 150 °C to allow the development of nanophase-separated structures. The kinetics of the structure formation is fast, largely due to the lack of chain entanglement at this low PS molecular weight.[84] Typically, it took less than 1 h to fully develop the ordered nanostructures, and prolonged annealing does not significantly improve the extent of nanophase separation. One-dimensional (1D) SAXS patterns of the thermally treated samples were then recorded at room temperature after the thermal treatment. Microtomed thin sections of the samples used in SAXS experiments were obtained for transmission electron microscopy (TEM) experiments.

Self-Assembly of the XPOSS-PS$_{35}$ Samples. DPOSS-PS$_{35}$, with a volume fraction of $f_{DPOSS} = 0.22$, is known to exhibit a DG phase,[75] as supported by the SAXS result in reciprocal space (Figure 1a) and the TEM bright-field image in real space (Figure 2a and Figure S11). The set of four scattering peaks with a q ratio of $\sqrt{6}:\sqrt{8}:\sqrt{20}:\sqrt{22}$ is characteristic of the DG phase with $Ia\bar{3}d$ symmetry.[85] Real space TEM image of the microtomed sample exhibits the typical pattern of the $(\bar{2}11)$ planes (Figure 2a) and the "wagon-wheel" like pattern along the [111] direction (Figure S11) of the DG morphology.[75,85] The d-spacing value corresponding to the first scattering peak d_1 is calculated from the q_1 value of the peak by $d_1 = 2\pi/q_1$, which equals 8.4 nm. The ability of DPOSS-PS giant surfactant to generate nanophase separation at such a small length scale is indicative that the interaction parameter χ between the DPOSS heads and PS tails is high enough to induce strong segregation, as supported by the temperature-resolved SAXS experiments (see below for details).
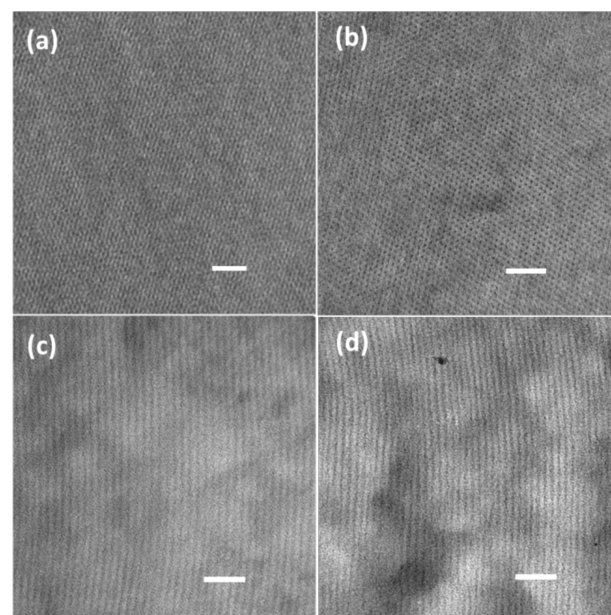

Figure 2. Bright-field TEM images of the microtomed samples. (a) The characteristic pattern of a DG phase along the [211] direction from DPOSS-PS$_{35}$; (b) hexagonally packed cylinders along the [0001] direction of the Hex phase; lamellae structures with a periodic spacing of ∼10 nm from F$_{17}$POSS-PS$_{35}$ as in (c) and ∼8.5 nm from F$_{13}$POSS-PS$_{35}$ as in (d). Images shown in (a) and (b) are obtained without staining, and the darker domains are composed of DPOSS and APOSS cages, respectively. Images shown in (c) and (d) are stained with RuO$_4$, and the darker lines are thus the PS domains. Scale bar: 50 nm.

When the periphery functional groups on the POSS heads are changed to seven carboxylic acids, a Hex phase is observed in the APOSS-PS$_{35}$ sample, as revealed by the set of three peaks with q ratio of $1:\sqrt{3}:2$ in the SAXS pattern (Figure 1b). The interplanar spacing d_1 calculated from q_1 is 7.6 nm. TEM bright-field image (Figure 2b) shows the hexagonally packed cylinders along the [0001] direction, with a measured interplanar d-spacing being also 7.6 ± 0.2 nm. With $f_{APOSS} = 0.21$, the APOSS heads should constitute the minor domains, which appeared darker in the TEM image (Figure 2b), while the PS tails form the matrix. Compared to DPOSS-PS$_{35}$ with $f_{DPOSS} = 0.22$, the APOSS heads in APOSS-PS$_{35}$ have a slightly lower $f_{APOSS} = 0.21$, and the PS tail molecular weights are identical. However, a SAXS pattern of another APOSS-PS$_{33}$ sample with $f_{APOSS} = 0.22$ also exhibits a Hex phase with a smaller $d_1 = 7.3$ nm (Figure S12). This result indicates that different thiol ligands on the POSS heads can result in different interactions and packing requirements and play an important role in determining the self-assembled nanostructures.[15,85,86]

Two thiol molecules with fluorinated alkyl chains of different lengths are selected to obtain larger XPOSS heads with high χ values, which may lead to the formation of Lam phase at the identical molecular weight of PS tails. Generally speaking, fluorinated materials have low surface energy and are immiscible with neither the aqueous phase nor the oil phase.[87,88] Our group has previously reported the synthesis of fluorinated POSS−polymer conjugates with one or two different polymer tails[72] and has recently reported the development of a "clickable" fluorinated POSS building block.[89] Our recent results have confirmed that the fluorinated POSS cages show strong segregation tendency with both
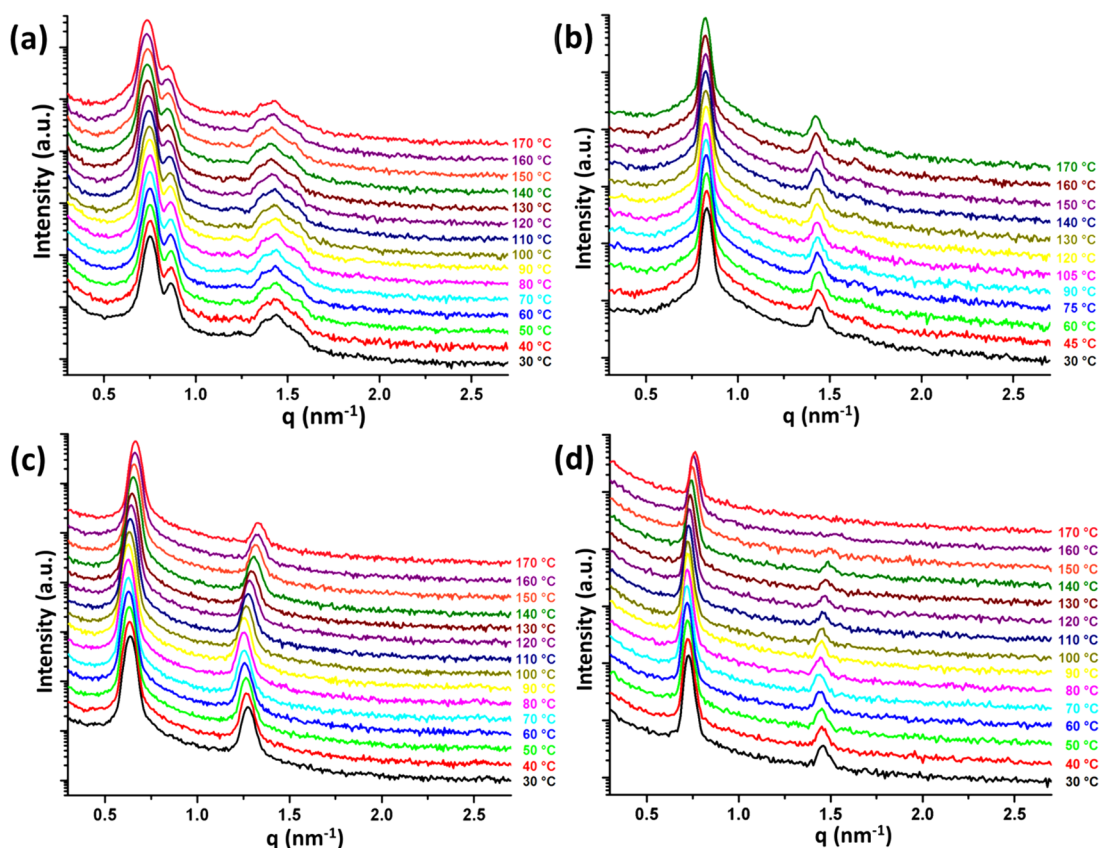
Figure 3. Temperature-resolved 1D SAXS patterns of (a) DPOSS-PS$_{35}$, (b) APOSS-PS$_{35}$, (c) F$_{17}$POSS-PS$_{35}$, and (d) F$_{13}$POSS-PS$_{35}$. The data are offset by a factor of 2 for clarity.

hydrophobic PS chains and hydrophilic poly(ethylene glycol) (PEO) chains.[78]

Both F$_{17}$POSS-PS$_{35}$ (f_{PS} = 0.63) and F$_{13}$POSS-PS$_{35}$ (f_{PS} = 0.68) indeed show Lam phases, as supported by the two sharp scattering peaks with a q ratio of 1:2 in the small-angle region (Figures 1c and 1d). The periodicity values of the lamellae calculated based on the SAXS results are 9.6 nm for F$_{17}$POSS-PS$_{35}$ and 8.5 nm for F$_{13}$POSS-PS$_{35}$. After staining with RuO$_4$, the alternating darker and lighter domains reveal by the real-space, bright-field TEM images provided a direct proof of the formation of Lam phase (Figures 2c and 2d). From the TEM image, the lamellar spacing in the F$_{17}$POSS-PS$_{35}$ sample is ~10 nm, while the F$_{17}$POSS domain is determined as ~3 nm, which agree well with the value calculated from the volume fractions. Interestingly, when a shorter fluorinated thiol ligand is used, the F$_{13}$POSS-PS$_{35}$ lamellae possess a smaller d-spacing of 8.5 nm (Figure 1d). Comparing with F$_{17}$POSS-PS$_{35}$, the decrease in d-spacing can be largely attributed to the shorter fluorinated alkyl chains.

It is worth mentioning that the nanophase-separated structures can only be achieved when a large enough driving force (χN) exists. Clearly, this prerequisite is satisfied in the cases of APOSS-PS$_{35}$, DPOSS-PS$_{35}$, F$_{17}$POSS-PS$_{35}$, and F$_{13}$POSS-PS$_{35}$. The effort to tune the interaction parameter by using 1-thiolpropanol as the ligand afforded HPPOSS-PS$_{35}$, however, fails to produce ordered phase under similar experimental conditions. The only scattering peak obtained from 1D SAXS pattern shows a relatively broad scattering intensity (Figure 1e). Comparing the structures of HPPOSS-PS$_{35}$ and APOSS-PS$_{35}$, it is evident that both POSS heads possess very close molecular weights (Table 1) but differ only

in several atoms in the functional groups. Nevertheless, the apparent interaction parameter χ turns out to be much smaller in the case of HPPOSS-PS. It is thus concluded that seven hydroxyl groups in the HPPOSS head generate smaller chemical incompatibility than the APOSS head that has seven carboxylic acid groups. On the other hand, DPOSS-PS$_{35}$ has seven more hydroxyl groups compared to HPPOSS-PS$_{35}$ and results in large enough interaction parameters to achieve nanophase separation under the condition of identical PS tail molecular weight. The fact that such small compositional difference between HPPOSS-PS$_{35}$ and APOSS-PS$_{35}$ can significantly change the interactions of the heads, and thus their self-assembled structures, clearly illustrates the exceptionally sensitive dependence of the self-assembly behaviors on the chemical compositions, even in a macromolecular system.

To qualitatively study the interaction parameters between the PS tails and the functionalized POSS heads, temperature-resolved SAXS experiments were performed (Figure 3). While the DPOSS-PS$_{35}$ and APOSS-PS$_{35}$ samples show negligible changes of the domain sizes (Figures 3a and 3b) upon heating, the d-spacings of the Lam phases from F$_{17}$POSS-PS$_{35}$ and F$_{13}$POSS-PS$_{35}$ samples exhibit first thermal expansion and then thermal shrinkage (Figures 3c and 3d). For F$_{17}$POSS-PS$_{35}$, the inflection temperature from the thermal expansion to thermal shrinkage takes place at ca. 80 °C (Figure S13, black curve), while for F$_{13}$POSS-PS$_{35}$ the inflection temperature is at ca. 70 °C (Figure S13, red curve). Below the inflection temperature, the observed d_1 increases with increasing temperature in the Lam structures for both F$_{17}$POSS-PS$_{35}$ and F$_{13}$POSS-PS$_{35}$ samples. This behavior is significantly different from the established behaviors of common neat diblock copolymers.[90,91]
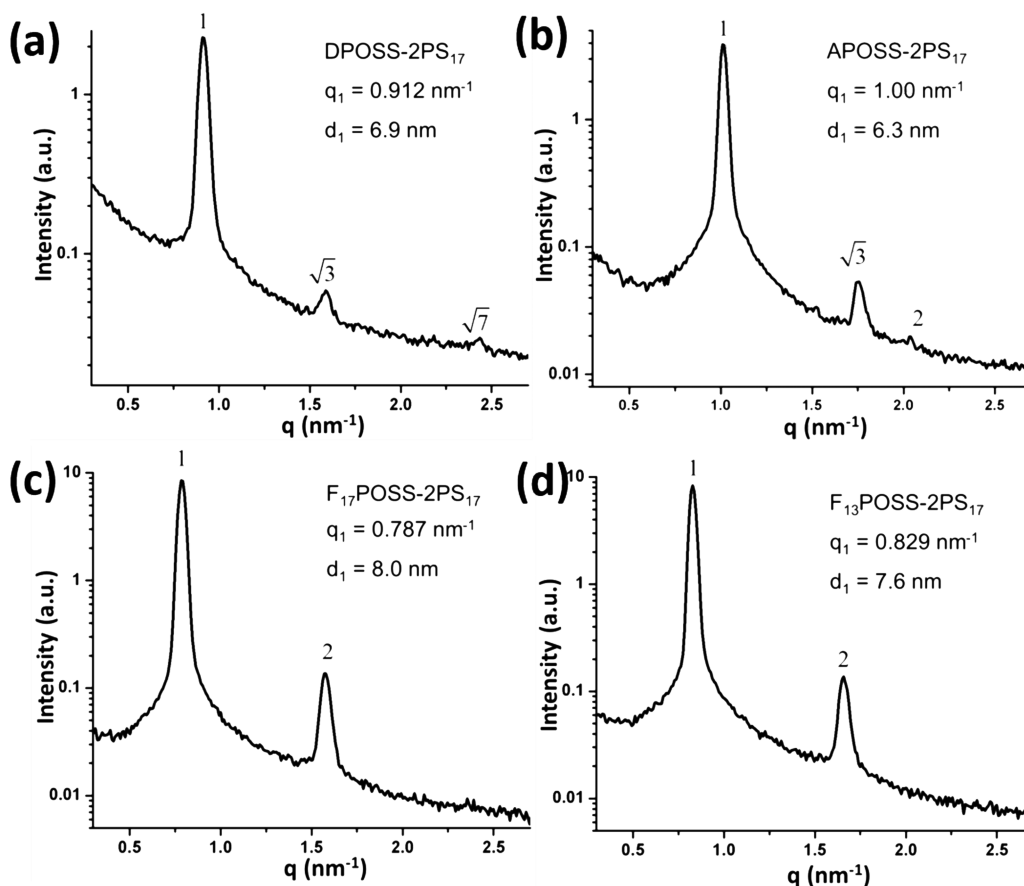
Figure 4. 1D SAXS patterns of (a) DPOSS-2PS$_{17}$, (b) APOSS-2PS$_{17}$, (c) F$_{17}$POSS-2PS$_{17}$, and (d) F$_{13}$POSS-2PS$_{17}$. Because of the topological variations, different self-assembled structures are observed when compared to their XPOSS-PS$_{35}$ topological isomers.

This unusual phenomenon might be attributed to the unique configurational change of the FPOSS heads[78] upon heating that is strikingly different from the flexible polymer chains of random-coil conformations.[90]

In addition, upon heating the F$_{17}$POSS-PS$_{35}$ and F$_{13}$POSS-PS$_{35}$ samples, the second-order peaks in SAXS gradually decrease in intensity and become very weak at 170 °C in the F$_{13}$POSS-PS$_{35}$ sample. However, plots of the full width at half-maximum (fwhm) and the intensity of the primary peak of the SAXS patterns as a function of temperature display no sudden changes in the tested temperature ranges (Figures S14 and S15), indicating that no order−disorder transition takes place up to 170 °C for all the four samples that form the nanophase-separated structures.[92,93] Although quantitative calculations of the interaction parameters are not available, these experimental results directly indicate that properly functionalized POSS heads show strong segregation tendency with the PS tails. This conclusion is based on the fact that the degree of polymerization of the PS tails is merely 35 repeating units, and the overall molecular weights of the giant surfactants are smaller than 8.0 kg/mol (see Table 1). Moreover, the temperature-dependent changes in SAXS patterns are fully reversible.

Self-Assembly of the XPOSS-2PS$_{17}$ Samples. XPOSS-2PS$_{17}$ giant surfactants have almost identical chemical compositions to the corresponding XPOSS-PS$_{35}$ samples but with different molecular architectures, which are referred as pairs of topological isomers. Therefore, the differences in self-assembly behaviors must be attributed to the topological effect.

A SAXS pattern of DPOSS-2PS$_{17}$ suggested a Hex phase, as revealed by the observation of three peaks with a q ratio of $1:\sqrt{3}:\sqrt{7}$ (Figure 4a), while its topological isomer DPOSS-PS$_{35}$ shows a DG phase. This comparison indicates that the phase boundary between the DG and Hex phases in the DPOSS-2PS$_n$ system shifts toward lower f_{PS}, as a result of the topological variation. Moreover, the calculated d_1 value from the primary scattering peak is 6.9 nm. In combination with $f_{DPOSS} = 0.22$, the calculated diameter of the DPOSS cylinders is 4.0 nm, matching well with the estimated value from the bright-field TEM image shown in Figure 5a.

Like APOSS-PS$_{35}$, APOSS-2PS$_{17}$ also shows a Hex phase after thermal annealing, as indicated by the scattering pattern with q values of peaks being $1:\sqrt{3}:2$. The bright-field TEM image in Figure 5b also confirmed the hexagonal packing of APOSS cylinders in the PS matrix. Remarkably, the d-spacing value corresponding to the primary scattering peak q_1 is calculated to be 6.3 nm, representing a 17% decrease compared to that from its topological isomer APOSS-PS$_{35}$ (7.6 nm). Decreased nanostructure feature size has also been reported in AB$_n$ oligosaccharide-containing block copolymers with multiple polymer tails compared with their linear AB counterparts with the same overall molecular weight.[32] The shape of a single giant surfactant packed into the Hex phase can be considered as a fan-shaped sector as a building block of the cylinder. Apparently, breaking the PS tail of APOSS-PS$_{35}$ into two shorter PS tails with a half length for each in APOSS-2PS$_{17}$ decreases the intercolumnar distances but increases the angle of the fan-shaped sector for each molecule (see below for details).
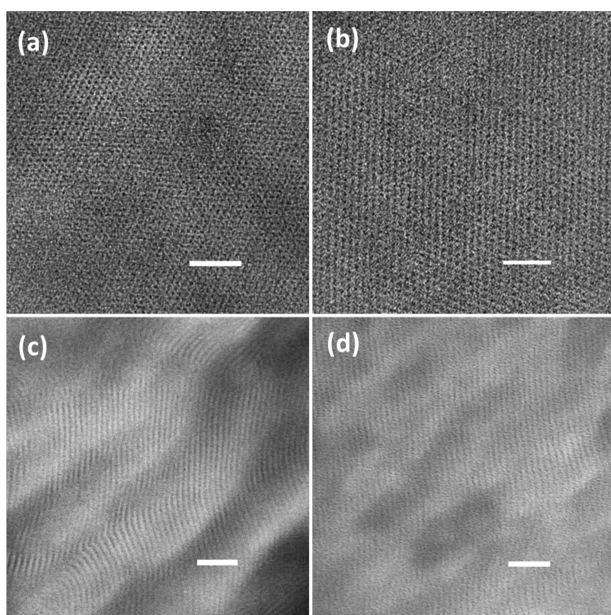
Figure 5. Bright-field TEM images of the microtomed XPOSS-2PS$_{17}$ samples. Hexagonally packed cylinders along the [0001] direction of the Hex phase from (a) DPOSS-2PS$_{17}$ and (b) APOSS-2PS$_{17}$. Lamellae structures with a periodic spacing of ~8 nm from F$_{17}$POSS-2PS$_{17}$ as in (c) and ~7.5 nm from F$_{13}$POSS-2PS$_{17}$ as in (d). Images shown in (a) and (b) are obtained without staining, and the darker domains are composed of DPOSS and APOSS cages, respectively. Images shown in (c) and (d) are stained with RuO$_4$, and the darker lines are thus the PS domains. Scale bar: 50 nm.

Therefore, tuning the molecular architecture provides a practical method to further decrease the feature sizes of phase-separated microdomains.[41]

Both F$_{17}$POSS-2PS$_{17}$ and F$_{13}$POSS-2PS$_{17}$ samples show Lam structures but with decreased lamellae periodicity. The SAXS patterns of F$_{17}$POSS-2PS$_{17}$ and F$_{13}$POSS-2PS$_{17}$ (Figures 4c and 4d) show two strong and sharp scattering peaks with a 1:2 q ratio, indicating the lamellar structures. After staining with RuO$_4$, bright-field TEM images of the microtomed samples show alternating gray and black lines, corresponding to the fluorinated POSS cages and the PS chains, respectively. The periodicity values for F$_{17}$POSS-2PS$_{17}$ and F$_{13}$POSS-2PS$_{17}$ are calculated as 8.0 and 7.6 nm, respectively, which are further reduced comparing to the values of 9.6 and 8.5 nm for F$_{17}$POSS-PS$_{35}$ and F$_{13}$POSS-PS$_{35}$, respectively. The decreased lamellar periodicity seems in agreement with the fact that F$_{17}$POSS-2PS$_{17}$ and F$_{13}$POSS-2PS$_{17}$ have two shorter PS chains than their topological isomers. Similar to the situation in the Hex region, the topological effect also results in reduced feature sizes of self-assembled nanostructures in the Lam region.

After thermal annealing at 150 °C, HPPOSS-2PS$_{17}$ with seven hydroxyl groups on the POSS cages failed to exhibit ordered nanostructures, as indicated by the observation of one broad scattering peak in SAXS pattern (Figure S16). This is again due to the weak chemical incompatibility between HPPOSS cages and PS chains that is not enough to drive nanophase separation.

Temperature-resolved SAXS experiments were also performed to check the thermal stability of the self-assembled nanostructures in these XPOSS-2PS$_{17}$ samples. Similar to the observations in APOSS-PS$_{35}$, scattering peaks from DPOSS-
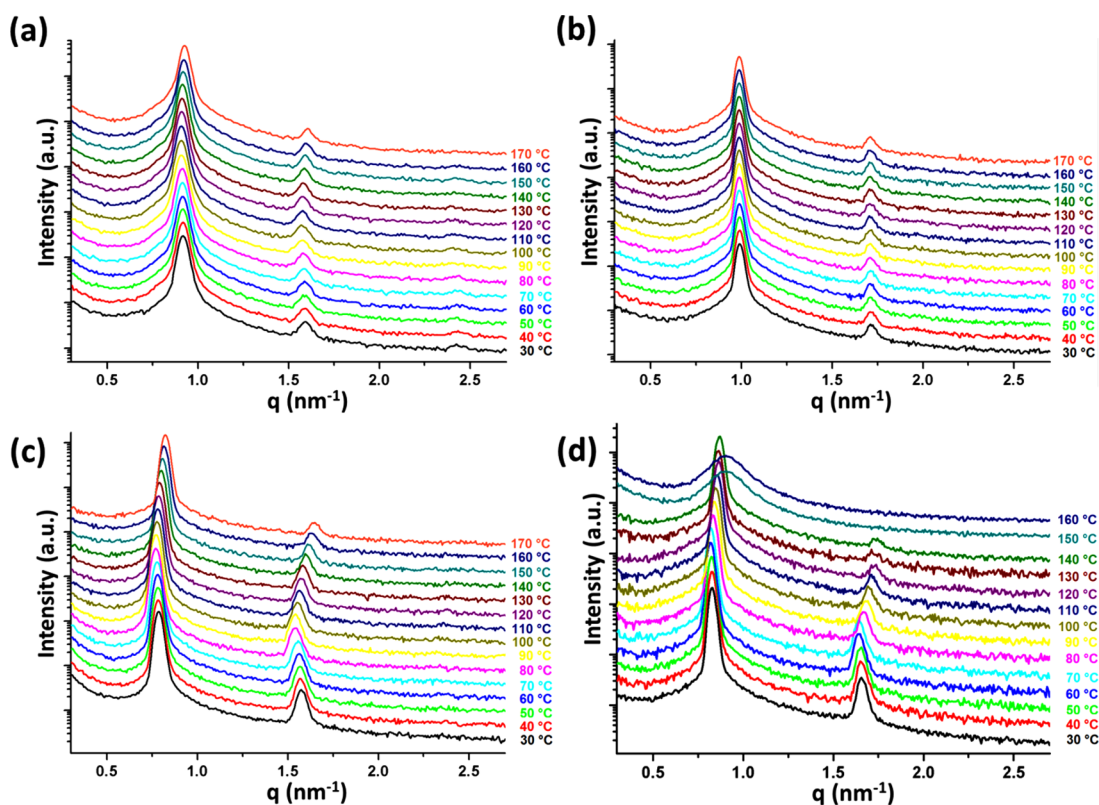

Figure 6. Temperature-resolved 1D SAXS patterns of (a) DPOSS-2PS$_{17}$, (b) APOSS-2PS$_{17}$, (c) F$_{17}$POSS-2PS$_{17}$, and (d) F$_{13}$POSS-2PS$_{17}$. The data are offset by a factor of 2 for clarity.

$2PS_{17}$ and $APOSS-2PS_{17}$ samples with Hex structures do not show significant temperature dependence in structural integrity and periodicity. Both of the Hex structures remain almost unchanged up to 170 °C. For $F_{17}POSS-2PS_{17}$ and $F_{13}POSS-2PS_{17}$ samples showing Lam structures, the thermal expansion to shrinkage transition is also observed. The inflection temperatures for $F_{17}POSS-2PS_{17}$ and $F_{13}POSS-2PS_{17}$ were again ca. 80 and 70 °C, respectively, suggesting that the phenomenon arises from the same origin of the fluorinated POSS cages as described above (Figure S17). More importantly, a sharp order−disorder transition (ODT) is identified in $F_{13}POSS-2PS_{17}$, as indicated by the disappearance of both scattering peak intensity above 140 °C, as well as by the sudden increase of fwhm of the primary peak in its SAXS pattern at above 140 °C (Figure S18), and the sudden drop of primary peak intensity in SAXS patterns at above 140 °C (Figure S19). Compared to $F_{17}POSS-2PS_{17}$, the lower ODT temperature of $F_{13}POSS-2PS_{17}$ can be explained by the shorter fluorinated alkyl chains and thus a smaller interaction parameter. The fact that no ODT was observed in $F_{13}POSS-PS_{35}$, however, can only be attributed to the molecular architecture difference between $F_{13}POSS-PS_{35}$ and $F_{13}POSS-2PS_{17}$. It should be noted that the ODT is thermally reversible. Upon cooling, the Lam structure with the same lamellae periodicity was formed again with fast kinetics.

Topological Effects between XPOSS-PS and XPOSS-2PS. By comparing the self-assembled nanostructures of the two model series of giant surfactants, significant topological effects on the self-assembly of POSS-based giant surfactants can be revealed. First, the comparison between $DPOSS-PS_{35}$ and $DPOSS-2PS_{17}$ suggested that phase boundaries between the commonly observed phases could be shifted by the molecular architectural change, which has been theoretically predicted in the AB_n miktoarm star copolymers.[50] This effect can be understood by analyzing the interfacial curvature between the self-assembled nanodomains.[41] When two shorter PS tails are tethered to a DPOSS cage instead of one longer PS tail, the increased cross-sectional area of the PS tails help create higher interfacial curvature inward toward the DPOSS domain, which further facilitates the transition from the DG phase to the Hex phase. In general, it indicates that by increasing the number of PS tails, formation of ordered structures with higher interfacial curvature becomes more favorable compared to the DPOSS-PS samples at the same f_{PS}. As a result, the Hex phase and BCC phase might be obtained at lower f_{PS} and thus lower PS molecular weights by designing giant surfactants with multiple tails, given the fixed overall molecular weight of one POSS head.

Second, the architectural change may also significantly influence the molecular packing configurations within the self-assembled nanostructures. For example, both of the topological isomers of $APOSS-PS_{35}$ and $APOSS-2PS_{17}$ show the Hex phase, although the latter has a smaller d_1 (Table 1). The radius of the APOSS cylinders (D_c) in the Hex phase can be calculated according to[79]

$$D_c = [(2f_{DPOSS}d_1{}^2)/(\sqrt{3}\pi)]^{1/2} \tag{1}$$

which gives 2.1 nm for $APOSS-PS_{35}$ and 1.7 nm for $APOSS-2PS_{17}$. Considering a stratum of the cylinders with a unit height $h = 1.0$ nm along the cylindrical long axis, the number of molecules packed in the stratum μ can be calculated by

$$\mu = \frac{2d_1{}^2h}{\sqrt{3}\,V_0}$$

$$= \frac{2d_1{}^2hN_A}{\sqrt{3}\,(M_{PS}/\rho_{PS} + M_{BPOSS}/\rho_{BPOSS} + M_{DPOSS}/\rho_{DPOSS})} \tag{2}$$

where V_0 is the volume of each molecule and N_A is the Avogadro constant. The calculated μ values for $APOSS-PS_{35}$ and $APOSS-2PS_{17}$ are 9.0 and 6.2, respectively. It is thus obvious that the planar angle of the fan-shaped sector occupied by each $APOSS-2PS_{17}$ molecule is larger than that of one $APOSS-PS_{35}$ molecule (58° versus 40°). Therefore, the $APOSS-2PS_{17}$ molecules packed in a looser manner, leading to reduced diameter of the APOSS cylindrical domains in order to keep the constant PS density.

Considering the relatively short PS tails, the molecular packing models in the Lam phases can be described by the double-layered packing of the giant surfactants with head-to-head arrangement of the POSS cages. The cross-sectional area A_0 corresponding to one molecule at the flat microdomain interfaces is thus calculated according to

$$A_0 = \frac{2M_{PS}}{\rho_{PS}N_A d_1 f_{PS}} \tag{3}$$

Calculated A_0 values for $F_{17}POSS-PS_{35}$ and $F_{13}POSS-PS_{35}$ are 1.9 and 2.0 nm², respectively. Interestingly, although the $F_{17}POSS$ cages are larger than the $F_{13}POSS$, a smaller A_0 is observed for $F_{17}POSS-PS_{35}$. As a result, the length of the PS_{35} tail along the normal direction of the lamellae in $F_{17}POSS-PS_{35}$ is 3.1 nm, which is larger than that in $F_{13}POSS-PS_{35}$ (2.9 nm). These results can be explained by the fact that $F_{17}POSS$ cages have a higher chemical incompatibility with the PS tails than the $F_{13}POSS$ cages do. Therefore, the PS tails in $F_{17}POSS-PS_{35}$ prefer to stretch to a larger extend to decrease the interfacial tension between the two immiscible domains.[78] The observed equilibrium PS chain length is determined by the balance between interfacial tension and PS stretching energy.

When it comes to $F_{17}POSS-2PS_{17}$ and $F_{13}POSS-2PS_{17}$, the calculated A_0 values according to eq 3 are 2.3 nm² for both samples. Attachment of two PS tails in $XPOSS-2PS_{17}$ samples results in increased A_0 values compared to their $XPOSS-PS_{35}$ counterparts. The fact that both $F_{17}POSS$ and $F_{13}POSS$ cages show the same A_0 values suggests that this area might be required to accommodate two PS chains at the interface. With an increased A_0 and fixed volume, the length of the POSS domains in the lamellae phase is further reduced, which also contributes to the decrease in overall lamellae periodicity of $F_{17}POSS-2PS_{17}$ and $F_{13}POSS-2PS_{17}$ compared to $F_{17}POSS-PS_{35}$ and $F_{13}POSS-PS_{35}$, in addition to the decreased PS tail length.

Estimation of the Effective χ Value. Another important observation in the topology-induced difference is the ODT recorded from $F_{13}POSS-2PS_{17}$, which is the only sample in these two series that shows such a transition at elevated temperature. The lower temperature for an ODT in $F_{13}POSS-2PS_{17}$ compared to $F_{13}POSS-PS_{35}$ reminds us with the predictions from the theoretical study of the AB_n systems.[50] In contrast to symmetric AB diblock copolymers with a critical $\chi N = 10.5$, the critical point for AB_2 copolymers is calculated as 13.5 using the mean-field approach. To further generalize, the critical transition point evolves to higher χN or lower temperatures as the asymmetry of AB_n copolymers increases

(as n increases).[50] Our observations of $F_{13}POSS\text{-}PS_{35}$ and $F_{13}POSS\text{-}2PS_{17}$ are qualitatively in agreement with this prediction. Assuming that the $\chi N = 13.5$ criterion works for $F_{13}POSS\text{-}2PS_{17}$, the estimated χ value at the ODT temperature (ca. 150 °C) is 0.185, using a reference volume, ν_0, of 118 Å^3 ($N = 73$ for $F_{13}POSS\text{-}2PS_{17}$; see Table 1). Qualitatively, this value is larger than many known high-χ diblock copolymer systems,[19,43] which allows further downsizing the feature size of the phase-separated domains. In fact, the periodicity d_1 values for $F_{17}POSS\text{-}2PS_{17}$ and $F_{13}POSS\text{-}2PS_{17}$ are 8.0 and 7.6 nm, respectively, which are quite close to the smallest feature sizes reported in a PS−PEO system doped with metal salts.[94] Moreover, it is obvious that APOSS, DPOSS, and $F_{17}POSS$ cages should have even higher χ values with PS tails than the $F_{13}POSS$ cages, indicating that the XPOSS-PS system provides an additional platform to design novel high-χ value block copolymer analogues for obtaining self-assembled nanostructures with sub-10 nm feature sizes.

CONCLUSION

In summary, two series of XPOSS-PS$_{35}$ and XPOSS-2PS$_{17}$ giant surfactants are prepared via one-step thiol−ene reaction from two common precursors VPOSS-PS$_{35}$ and VPOSS-2PS$_{17}$, which have almost identical chemical compositions and molecular weights. By introducing different functional groups onto the POSS heads, we have demonstrated that the self-assembled morphology from the resulting giant surfactants sensitively depends on the molecular details of the periphery functional groups of the POSS cages and the molecular topology. Specifically, the different XPOSS heads tune the volume fractions and interaction parameters, leading to various nanophase separated structures with sub-10 nm feature sizes, as proved by combined SAXS and TEM techniques. When comparing XPOSS-PS$_{35}$ and XPOSS-2PS$_{17}$ with the same XPOSS heads, it is revealed that the topological change of having two short tails will result in shifted phase boundaries toward lower f_{PS}, reduced feature sizes, and different molecular packing configurations. Moreover, thermal stability of the self-assembled structures is studied by temperature-resolved SAXS experiments. Although most samples fail to show ODT up to 170 °C, a disordered phase is observed for $F_{13}POSS\text{-}2PS_{17}$ at above 140 °C. The reduced ODT temperature of $F_{13}POSS\text{-}2PS_{17}$ can also be attributed to the topological variance. The estimated χ value for $F_{13}POSS\text{-}2PS_{17}$ at $T = 150$ °C and $\nu_0 = 118$ Å^3 is 0.185, which may be the lower minimum of these two series of giant surfactants, but is higher than many reported diblock copolymers. These results demonstrated that our POSS-based giant surfactants offer a practical and precisely controllable approach to engineer self-assembled nanostructures at the sub-10 nm length scale.

The study also has general implications in tuning self-assembled structures with molecular precision by combining the following strategies: (i) introducing functional thiol ligands other than those tested here; (ii) controlling the molecular weight of the PS tail attached to the POSS cage;[75] (iii) tuning the molecular architecture of the giant surfactants (such as giant lipids,[70] giant gemini surfactants,[69,74] multiheaded giant surfactants,[69,75] and others[95,96]); and (iv) changing the compositions of the polymer building blocks.[70,74] Systematic variations of these structural and topological parameters would afford self-assembled nanostructures with controlled symmetry and domain sizes.

ASSOCIATED CONTENT

ⓈSupporting Information

The Supporting Information is available free of charge on the ACS Publications website at DOI: 10.1021/acs.macromol.6b02446.

    Additional characterization data (PDF)

AUTHOR INFORMATION

Corresponding Authors

*E-mail scheng@uakron.edu (S.Z.D.C.).
*E-mail wenbin@pku.edu.cn (W.-B.Z.).
*E-mail shi@mcmaster.ca (A.-C.S.).

ORCID

Stephen Z. D. Cheng: 0000-0003-1448-0546

Notes

The authors declare no competing financial interest.

REFERENCES

(1) Whitesides, G. M.; Grzybowski, B. Self-assembly at all scales. *Science* **2002**, *295*, 2418−2421.

(2) Whitesides, G. M.; Boncheva, M. Beyond molecules: Self-assembly of mesoscopic and macroscopic components. *Proc. Natl. Acad. Sci. U. S. A.* **2002**, *99*, 4769−4774.

(3) Fujita, M.; Oguro, D.; Miyazawa, M.; Oka, H.; Yamaguchi, K.; Ogura, K. Self-Assembly of 10 Molecules into Nanometer-Sized Organic Host Frameworks. *Nature* **1995**, *378*, 469−471.

(4) Stang, P. J.; Olenyuk, B. Self-Assembly, Symmetry, and Molecular Architecture: Coordination as the Motif in the Rational Design of Supramolecular Metallacyclic Polygons and Polyhedra. *Acc. Chem. Res.* **1997**, *30*, 502−518.

(5) Hartgerink, J. D.; Beniash, E.; Stupp, S. I. Self-Assembly and Mineralization of Peptide-Amphiphile Nanofibers. *Science* **2001**, *294*, 1684−1688.

(6) Zhang, L.; Eisenberg, A. Multiple Morphologies of "Crew-Cut" Aggregates of Polystyrene-b-poly(acrylic acid) Block Copolymers. *Science* **1995**, *268*, 1728−1731.

(7) Cheng, S. Z. D. Design and engineering of polymer/macromolecular structures on the 2−100 nm length scale: A personal view on structural research. *J. Polym. Sci., Part B: Polym. Phys.* **2005**, *43*, 3361−3364.

(8) Ruiz, R.; Sandstrom, R. L.; Black, C. T. Induced Orientational Order in Symmetric Diblock Copolymer Thin Films. *Adv. Mater.* **2007**, *19*, 587−591.

(9) Black, C. T.; Ruiz, R.; Breyta, G.; Cheng, J. Y.; Colburn, M. E.; Guarini, K. W.; Kim, H. C.; Zhang, Y. Polymer self assembly in semiconductor microelectronics. *IBM J. Res. Dev.* **2007**, *51*, 605−633.

(10) Hawker, C. J.; Russell, T. P. Block Copolymer Lithography: Merging "Bottom-Up" with "Top-Down" Processes. *MRS Bull.* **2005**, *30*, 952−966.

(11) Lin, B. J. Immersion lithography and its impact on semiconductor manufacturing. *J. Micro/Nanolithogr., MEMS, MOEMS* **2004**, *3*, 377−395.

(12) Kim, H.-C.; Park, S.-M.; Hinsberg, W. D. Block Copolymer Based Nanostructures: Materials, Processes, and Applications to Electronics. *Chem. Rev.* **2009**, *110*, 146−177.

(13) Tang, C.; Lennon, E. M.; Fredrickson, G. H.; Kramer, E. J.; Hawker, C. J. Evolution of Block Copolymer Lithography to Highly Ordered Square Arrays. *Science* **2008**, *322*, 429−432.

(14) Bates, C. M.; Maher, M. J.; Janes, D. W.; Ellison, C. J.; Willson, C. G. Block Copolymer Lithography. *Macromolecules* **2013**, *47*, 2−12.

(15) Bates, F. S.; Fredrickson, G. H. Block Copolymer Thermodynamics: Theory and Experiment. *Annu. Rev. Phys. Chem.* **1990**, *41*, 525−557.

(16) Almdal, K.; Koppi, K. A.; Bates, F. S.; Mortensen, K. Multiple ordered phases in a block copolymer melt. *Macromolecules* **1992**, *25*, 1743−1751.

(17) Bates, F. S.; Fredrickson, G. H. Block Copolymers—Designer Soft Materials. *Phys. Today* **1999**, *52*, 32−38.

(18) Bates, F. S. Polymer-Polymer Phase Behavior. *Science* **1991**, *251*, 898−905.

(19) Sinturel, C.; Bates, F. S.; Hillmyer, M. A. High χ−Low N Block Polymers: How Far Can We Go? *ACS Macro Lett.* **2015**, *4*, 1044−1050.

(20) Jung, Y. S.; Chang, J. B.; Verploegen, E.; Berggren, K. K.; Ross, C. A. A Path to Ultranarrow Patterns Using Self-Assembled Lithography. *Nano Lett.* **2010**, *10*, 1000−1005.

(21) Son, J. G.; Gotrik, K. W.; Ross, C. A. High-Aspect-Ratio Perpendicular Orientation of PS-b-PDMS Thin Films under Solvent Annealing. *ACS Macro Lett.* **2012**, *1*, 1279−1284.

(22) Girardot, C.; Böhme, S.; Archambault, S.; Salaün, M.; Latu-Romain, E.; Cunge, G.; Joubert, O.; Zelsmann, M. Pulsed Transfer Etching of PS−PDMS Block Copolymers Self-Assembled in 193 nm Lithography Stacks. *ACS Appl. Mater. Interfaces* **2014**, *6*, 16276−16282.

(23) Kathrein, C. C.; Bai, W.; Currivan-Incorvia, J. A.; Liontos, G.; Ntetsikas, K.; Avgeropoulos, A.; Böker, A.; Tsarkova, L.; Ross, C. A. Combining Graphoepitaxy and Electric Fields toward Uniaxial Alignment of Solvent-Annealed Polystyrene−b−Poly-(dimethylsiloxane) Block Copolymers. *Chem. Mater.* **2015**, *27*, 6890−6898.

(24) Jeong, J. W.; Park, W. I.; Kim, M.-J.; Ross, C. A.; Jung, Y. S. Highly Tunable Self-Assembled Nanostructures from a Poly(2-vinylpyridine-b-dimethylsiloxane) Block Copolymer. *Nano Lett.* **2011**, *11*, 4095−4101.

(25) Bates, C. M.; Seshimo, T.; Maher, M. J.; Durand, W. J.; Cushen, J. D.; Dean, L. M.; Blachut, G.; Ellison, C. J.; Willson, C. G. Polarity-Switching Top Coats Enable Orientation of Sub−10-nm Block Copolymer Domains. *Science* **2012**, *338*, 775−779.

(26) Luo, Y.; Montarnal, D.; Kim, S.; Shi, W.; Barteau, K. P.; Pester, C. W.; Hustad, P. D.; Christianson, M. D.; Fredrickson, G. H.; Kramer, E. J.; Hawker, C. J. Poly(dimethylsiloxane-b-methyl methacrylate): A Promising Candidate for Sub-10 nm Patterning. *Macromolecules* **2015**, *48*, 3422−3430.

(27) Keen, I.; Yu, A.; Cheng, H.-H.; Jack, K. S.; Nicholson, T. M.; Whittaker, A. K.; Blakey, I. Control of the Orientation of Symmetric Poly(styrene)-*block*-poly(d,l-lactide) Block Copolymers Using Statistical Copolymers of Dissimilar Composition. *Langmuir* **2012**, *28*, 15876−15888.

(28) Rodwogin, M. D.; Spanjers, C. S.; Leighton, C.; Hillmyer, M. A. Polylactide−Poly(dimethylsiloxane)−Polylactide Triblock Copolymers as Multifunctional Materials for Nanolithographic Applications. *ACS Nano* **2010**, *4*, 725−732.

(29) Yao, L.; Oquendo, L. E.; Schulze, M. W.; Lewis, R. M.; Gladfelter, W. L.; Hillmyer, M. A. Poly(cyclohexylethylene)-*block*-Poly(lactide) Oligomers for Ultrasmall Nanopatterning Using Atomic Layer Deposition. *ACS Appl. Mater. Interfaces* **2016**, *8*, 7431−7439.

(30) Cushen, J. D.; Bates, C. M.; Rausch, E. L.; Dean, L. M.; Zhou, S. X.; Willson, C. G.; Ellison, C. J. Thin Film Self-Assembly of Poly(trimethylsilylstyrene-b-d,l-lactide) with Sub-10 nm Domains. *Macromolecules* **2012**, *45*, 8722−8728.

(31) Cushen, J. D.; Otsuka, I.; Bates, C. M.; Halila, S.; Fort, S.; Rochas, C.; Easley, J. A.; Rausch, E. L.; Thio, A.; Borsali, R.; Willson, C. G.; Ellison, C. J. Oligosaccharide/Silicon-Containing Block Copolymers with 5 nm Features for Lithographic Applications. *ACS Nano* **2012**, *6*, 3424−3433.

(32) Isono, T.; Otsuka, I.; Kondo, Y.; Halila, S.; Fort, S.; Rochas, C.; Satoh, T.; Borsali, R.; Kakuchi, T. Sub-10 nm Nano-Organization in AB2- and AB3-Type Miktoarm Star Copolymers Consisting of Maltoheptaose and Polycaprolactone. *Macromolecules* **2013**, *46*, 1461−1469.

(33) Isono, T.; Otsuka, I.; Suemasa, D.; Rochas, C.; Satoh, T.; Borsali, R.; Kakuchi, T. Synthesis, Self-Assembly, and Thermal Caramelization of Maltoheptaose-Conjugated Polycaprolactones Leading to Spherical, Cylindrical, and Lamellar Morphologies. *Macromolecules* **2013**, *46*, 8932−8940.

(34) Otsuka, I.; Osaka, M.; Sakai, Y.; Travelet, C.; Putaux, J.-L.; Borsali, R. Self-Assembly of Maltoheptaose-*block*-Polystyrene into Micellar Nanoparticles and Encapsulation of Gold Nanoparticles. *Langmuir* **2013**, *29*, 15224−15230.

(35) Otsuka, I.; Zhang, Y.; Isono, T.; Rochas, C.; Kakuchi, T.; Satoh, T.; Borsali, R. Sub-10 nm Scale Nanostructures in Self-Organized Linear Di- and Triblock Copolymers and Miktoarm Star Copolymers Consisting of Maltoheptaose and Polystyrene. *Macromolecules* **2015**, *48*, 1509−1517.

(36) Hirai, T.; Leolukman, M.; Jin, S.; Goseki, R.; Ishida, Y.; Kakimoto, M.-A.; Hayakawa, T.; Ree, M.; Gopalan, P. Hierarchical Self-Assembled Structures from POSS-Containing Block Copolymers Synthesized by Living Anionic Polymerization. *Macromolecules* **2009**, *42*, 8835−8843.

(37) Hirai, T.; Leolukman, M.; Liu, C. C.; Han, E.; Kim, Y. J.; Ishida, Y.; Hayakawa, T.; Kakimoto, M.; Nealey, P. F.; Gopalan, P. One-Step Direct-Patterning Template Utilizing Self-Assembly of POSS-Containing Block Copolymers. *Adv. Mater.* **2009**, *21*, 4334−4338.

(38) Ahn, B.; Hirai, T.; Jin, S.; Rho, Y.; Kim, K.-W.; Kakimoto, M.-A.; Gopalan, P.; Hayakawa, T.; Ree, M. Hierarchical Structure in Nanoscale Thin Films of a Poly(styrene-b- methacrylate grafted with POSS) (PS214-b-PMAPOSS27). *Macromolecules* **2010**, *43*, 10568−10581.

(39) Tada, Y.; Yoshida, H.; Ishida, Y.; Hirai, T.; Bosworth, J. K.; Dobisz, E.; Ruiz, R.; Takenaka, M.; Hayakawa, T.; Hasegawa, H. Directed Self-Assembly of POSS Containing Block Copolymer on Lithographically Defined Chemical Template with Morphology Control by Solvent Vapor. *Macromolecules* **2011**, *45*, 292−304.

(40) Tada, Y.; Yoshida, H.; Ishida, Y.; Hirai, T.; Bosworth, J. K.; Dobisz, E.; Ruiz, R.; Takenaka, M.; Hayakawa, T.; Hasegawa, H. Directed Self-Assembly of POSS Containing Block Copolymer on Lithographically Defined Chemical Template with Morphology Control by Solvent Vapor. *Macromolecules* **2012**, *45*, 292−304.

(41) Goseki, R.; Hirao, A.; Kakimoto, M.-A.; Hayakawa, T. Cylindrical Nanostructure of Rigid-Rod POSS-Containing Polymethacrylate from a Star-Branched Block Copolymer. *ACS Macro Lett.* **2013**, *2*, 625−629.

(42) Kennemur, J. G.; Hillmyer, M. A.; Bates, F. S. Synthesis, Thermodynamics, and Dynamics of Poly(4-tert-butylstyrene-b-methyl methacrylate). *Macromolecules* **2012**, *45*, 7228−7236.

(43) Kennemur, J. G.; Yao, L.; Bates, F. S.; Hillmyer, M. A. Sub-5 nm Domains in Ordered Poly(cyclohexylethylene)-*block*-poly(methyl methacrylate) Block Polymers for Lithography. *Macromolecules* **2014**, *47*, 1411−1418.

(44) Sweat, D. P.; Kim, M.; Larson, S. R.; Choi, J. W.; Choo, Y.; Osuji, C. O.; Gopalan, P. Rational Design of a Block Copolymer with a High Interaction Parameter. *Macromolecules* **2014**, *47*, 6687−6696.

(45) Maher, M. J.; Mori, K.; Sirard, S. M.; Dinhobl, A. M.; Bates, C. M.; Gurer, E.; Blachut, G.; Lane, A. P.; Durand, W. J.; Carlson, M. C.; Strahan, J. R.; Ellison, C. J.; Willson, C. G. Pattern Transfer of Sub-10 nm Features via Tin-Containing Block Copolymers. *ACS Macro Lett.* **2016**, *5*, 391−395.

(46) Carter, M. C. D.; Jennings, J.; Speetjens, F. W.; Lynn, D. M.; Mahanthappa, M. K. A Reactive Platform Approach for the Rapid Synthesis and Discovery of High χ/Low N Block Polymers. *Macromolecules* **2016**, *49*, 6268−6276.

(47) Mavroudis, A.; Avgeropoulos, A.; Hadjichristidis, N.; Thomas, E. L.; Lohse, D. J. Synthesis and Morphological Behavior of Model Linear and Miktoarm Star Copolymers of 2-Methyl-1,3-Pentadiene and Styrene. *Chem. Mater.* **2003**, *15*, 1976−1983.

(48) Khanna, K.; Varshney, S.; Kakkar, A. Miktoarm star polymers: advances in synthesis, self-assembly, and applications. *Polym. Chem.* **2010**, *1*, 1171−1185.

(49) Grason, G.; DiDonna, B.; Kamien, R. Geometric Theory of Diblock Copolymer Phases. *Phys. Rev. Lett.* **2003**, *91*, 058304.

(50) Grason, G. M.; Kamien, R. D. Interfaces in Diblocks: A Study of Miktoarm Star Copolymers. *Macromolecules* **2004**, *37*, 7371−7380.

(51) Matsen, M. W. Effect of Architecture on the Phase Behavior of AB-Type Block Copolymer Melts. *Macromolecules* **2012**, *45*, 2161−2165.

(52) Poelma, J. E.; Ono, K.; Miyajima, D.; Aida, T.; Satoh, K.; Hawker, C. J. Cyclic Block Copolymers for Controlling Feature Sizes in Block Copolymer Lithography. *ACS Nano* **2012**, *6*, 10845−10854.

(53) Shi, W.; Tateishi, Y.; Li, W.; Hawker, C. J.; Fredrickson, G. H.; Kramer, E. J. Producing Small Domain Features Using Miktoarm Block Copolymers with Large Interaction Parameters. *ACS Macro Lett.* **2015**, *4*, 1287−1292.

(54) Minehara, H.; Pitet, L. M.; Kim, S.; Zha, R. H.; Meijer, E. W.; Hawker, C. J. Branched Block Copolymers for Tuning of Morphology and Feature Size in Thin Film Nanolithography. *Macromolecules* **2016**, *49*, 2318−2326.

(55) Zhang, W.-B.; Yu, X.; Wang, C.-L.; Sun, H.-J.; Hsieh, I. F.; Li, Y.; Dong, X.-H.; Yue, K.; Van Horn, R.; Cheng, S. Z. D. Molecular Nanoparticles Are Unique Elements for Macromolecular Science: From "Nanoatoms" to Giant Molecules. *Macromolecules* **2014**, *47*, 1221−1239.

(56) Kuo, S.-W.; Chang, F.-C. POSS related polymer nano-composites. *Prog. Polym. Sci.* **2011**, *36*, 1649−1696.

(57) Zhang, W.; Müller, A. H. E. A "Click Chemistry" Approach to Linear and Star-Shaped Telechelic POSS-Containing Hybrid Polymers. *Macromolecules* **2010**, *43*, 3148−3152.

(58) Zhang, W.; Fang, B.; Walther, A.; Müller, A. H. E. Synthesis via RAFT Polymerization of Tadpole-Shaped Organic/Inorganic Hybrid Poly(acrylic acid) Containing Polyhedral Oligomeric Silsesquioxane (POSS) and Their Self-assembly in Water. *Macromolecules* **2009**, *42*, 2563−2569.

(59) Cardoen, G.; Coughlin, E. B. Hemi-Telechelic Polystyrene-POSS Copolymers as Model Systems for the Study of Well-Defined Inorganic/Organic Hybrid Materials. *Macromolecules* **2004**, *37*, 5123−5126.

(60) Baney, R. H.; Itoh, M.; Sakakibara, A.; Suzuki, T. Silsesquioxanes. *Chem. Rev.* **1995**, *95*, 1409−1430.

(61) Cordes, D.; Lickiss, P.; Rataboul, F. Recent Developments in the Chemistry of Cubic Polyhedral Oligosilsesquioxanes. *Chem. Rev.* **2010**, *110*, 2081−2173.

(62) Laine, R. M. Nanobuilding blocks based on the [OSiO1.5] (x = 6, 8, 10) octasilsesquioxanes. *J. Mater. Chem.* **2005**, *15*, 3725−3744.

(63) Roll, M. F.; Asuncion, M. Z.; Kampf, J.; Laine, R. M. para-Octaiodophenylsilsesquioxane, [p-IC6H4SiO1.5]8, a Nearly Perfect Nano-Building Block. *ACS Nano* **2008**, *2*, 320−326.

(64) Kroto, H. W.; Heath, J. R.; O'Brien, S. C.; Curl, R. F.; Smalley, R. E. C-60 - Buckminsterfullerene. *Nature* **1985**, *318*, 162−163.

(65) Yu, X.; Zhang, W.-B.; Yue, K.; Li, X.; Liu, H.; Xin, Y.; Wang, C.-L.; Wesdemiotis, C.; Cheng, S. Z. D. Giant Molecular Shape Amphiphiles Based on Polystyrene-Hydrophilic [60]Fullerene Conjugates: Click Synthesis, Solution Self-Assembly, and Phase Behavior. *J. Am. Chem. Soc.* **2012**, *134*, 7780−7787.

(66) Hirsch, A.; Vostrowsky, O. C-60 hexakisadducts with an octahedral addition pattern - A new structure motif in organic chemistry. *Eur. J. Org. Chem.* **2001**, *2001*, 829−848.

(67) Hirsch, A. Amphiphilic architectures based on fullerene and calixarene platforms: From buckysomes to shape-persistent micelles. *Pure Appl. Chem.* **2008**, *80*, 571−587.

(68) Yue, K.; Liu, C.; Guo, K.; Yu, X.; Huang, M.; Li, Y.; Wesdemiotis, C.; Cheng, S. Z. D.; Zhang, W.-B. Sequential "Click" Approach to Polyhedral Oligomeric Silsesquioxane-Based Shape Amphiphiles. *Macromolecules* **2012**, *45*, 8126−8134.

(69) Yue, K.; Liu, C.; Guo, K.; Wu, K.; Dong, X.-H.; Liu, H.; Huang, M.; Wesdemiotis, C.; Cheng, S. Z. D.; Zhang, W.-B. Exploring shape amphiphiles beyond giant surfactants: molecular design and click synthesis. *Polym. Chem.* **2013**, *4*, 1056−1067.

(70) Yue, K.; He, J.; Liu, C.; Huang, M.; Dong, X.-H.; Guo, K.; Ni, P.; Wesdemiotis, C.; Quirk, R.; Cheng, S. D.; Zhang, W.-B. Anionic synthesis of a "clickable" middle-chain azidefunctionalized polystyrene and its application in shape amphiphiles. *Chin. J. Polym. Sci.* **2013**, *31*, 71−82.

(71) Huang, M.; Hsu, C.-H.; Wang, J.; Mei, S.; Dong, X.; Li, Y.; Li, M.; Liu, H.; Zhang, W.; Aida, T.; Zhang, W.-B.; Yue, K.; Cheng, S. Z. D. Selective assemblies of giant tetrahedra via precisely controlled positional interactions. *Science* **2015**, *348*, 424−428.

(72) He, J.; Yue, K.; Liu, Y.; Yu, X.; Ni, P.; Cavicchi, K. A.; Quirk, R. P.; Chen, E.-Q.; Cheng, S. Z. D.; Zhang, W.-B. Fluorinated polyhedral oligomeric silsesquioxane-based shape amphiphiles: molecular design, topological variation, and facile synthesis. *Polym. Chem.* **2012**, *3*, 2112−2120.

(73) Yu, X.; Zhong, S.; Li, X.; Tu, Y.; Yang, S.; Van Horn, R.; Ni, C. Y.; Pochan, D. J.; Quirk, R. P.; Wesdemiotis, C.; Zhang, W.-B.; Cheng, S. Z. D. A Giant Surfactant of Polystyrene-(Carboxylic Acid-Functionalized Polyhedral Oligomeric Silsesquioxane) Amphiphile with Highly Stretched Polystyrene Tails in Micellar Assemblies. *J. Am. Chem. Soc.* **2010**, *132*, 16741−16744.

(74) Wang, Z.; Li, Y.; Dong, X.-H.; Yu, X.; Guo, K.; Su, H.; Yue, K.; Wesdemiotis, C.; Cheng, S. Z. D.; Zhang, W.-B. Giant gemini surfactants based on polystyrene-hydrophilic polyhedral oligomeric silsesquioxane shape amphiphiles: sequential "click" chemistry and solution self-assembly. *Chem. Sci.* **2013**, *4*, 1345−1352.

(75) Yu, X.; Yue, K.; Hsieh, I.-F.; Li, Y.; Dong, X.-H.; Liu, C.; Xin, Y.; Wang, H.-F.; Shi, A.-C.; Newkome, G. R.; Ho, R.-M.; Chen, E.-Q.; Zhang, W.-B.; Cheng, S. Z. D. Giant surfactants provide a versatile platform for sub-10-nm nanostructure engineering. *Proc. Natl. Acad. Sci. U. S. A.* **2013**, *110*, 10078−10083.

(76) Hsu, C. H.; Dong, X. H.; Lin, Z.; Ni, B.; Lu, P.; Jiang, Z.; Tian, D.; Shi, A. C.; Thomas, E. L.; Cheng, S. Z. Tunable Affinity and Molecular Architecture Lead to Diverse Self-Assembled Supramolecular Structures in Thin Films. *ACS Nano* **2016**, *10*, 919−929.

(77) Lin, Z.; Lu, P.; Hsu, C.-H.; Sun, J.; Zhou, Y.; Huang, M.; Yue, K.; Ni, B.; Dong, X.-H.; Li, X.; Zhang, W.-B.; Yu, X.; Cheng, S. Z. D. Hydrogen-Bonding-Induced Nanophase Separation in Giant Surfactants Consisting of Hydrophilic [60]Fullerene Tethered to Block Copolymers at Different Locations. *Macromolecules* **2015**, *48*, 5496−5503.

(78) Dong, X.-H.; Ni, B.; Huang, M.; Hsu, C.-H.; Chen, Z.; Lin, Z.; Zhang, W.-B.; Shi, A.-C.; Cheng, S. Z. D. Chain Overcrowding Induced Phase Separation and Hierarchical Structure Formation in Fluorinated Polyhedral Oligomeric Silsesquioxane (FPOSS)-Based Giant Surfactants. *Macromolecules* **2015**, *48*, 7172−7179.

(79) Wu, K.; Huang, M.; Yue, K.; Liu, C.; Lin, Z.; Liu, H.; Zhang, W.; Hsu, C.-H.; Shi, A.-C.; Zhang, W.-B.; Cheng, S. Z. D. Asymmetric Giant "Bolaform-like" Surfactants: Precise Synthesis, Phase Diagram, and Crystallization-Induced Phase Separation. *Macromolecules* **2014**, *47*, 4622−4633.

(80) Hoyle, C. E.; Lowe, A. B.; Bowman, C. N. Thiol-click chemistry: a multifaceted toolbox for small molecule and polymer synthesis. *Chem. Soc. Rev.* **2010**, *39*, 1355−1387.

(81) Hoyle, C. E.; Bowman, C. N. Thiol-Ene Click Chemistry. *Angew. Chem., Int. Ed.* **2010**, *49*, 1540−1573.

(82) Xi, W.; Scott, T. F.; Kloxin, C. J.; Bowman, C. N. Click Chemistry in Materials Science. *Adv. Funct. Mater.* **2014**, *24*, 2572−2590.

(83) Zhang, S.; Zou, J.; Zhang, F.; Elsabahy, M.; Felder, S. E.; Zhu, J.; Pochan, D. J.; Wooley, K. L. Rapid and Versatile Construction of Diverse and Functional Nanostructures Derived from a Polyphosphoester-Based Biomimetic Block Copolymer System. *J. Am. Chem. Soc.* **2012**, *134*, 18467−18474.

(84) Fetters, L. J.; Lohse, D. J.; Graessley, W. W. Chain dimensions and entanglement spacings in dense macromolecular systems. *J. Polym. Sci., Part B: Polym. Phys.* **1999**, *37*, 1023−1033.

(85) Vukovic, I.; Voortman, T. P.; Merino, D. H.; Portale, G.; Hiekkataipale, P.; Ruokolainen, J.; ten Brinke, G.; Loos, K. Double Gyroid Network Morphology in Supramolecular Diblock Copolymer Complexes. *Macromolecules* **2012**, *45*, 3503−3512.

(86) Cochran, E. W.; Garcia-Cervera, C. J.; Fredrickson, G. H. Stability of the Gyroid Phase in Diblock Copolymers at Strong Segregation. Volume 39, Number 7, March, 14, 2006, pp 2449−2451. *Macromolecules* **2006**, *39*, 4264−4264.

(87) de Wolf, E.; van Koten, G.; Deelman, B.-J. Fluorous phase separation techniques in catalysis. *Chem. Soc. Rev.* **1999**, *28*, 37−41.

(88) Zhang, W. Green chemistry aspects of fluorous techniques-opportunities and challenges for small-scale organic synthesis. *Green Chem.* **2009**, *11*, 911−920.

(89) Ni, B.; Dong, X.-H.; Chen, Z.; Lin, Z.; Li, Y.; Huang, M.; Fu, Q.; Cheng, S. Z. D.; Zhang, W.-B. "Clicking" fluorinated polyhedral oligomeric silsesquioxane onto polymers: a modular approach toward shape amphiphiles with fluorous molecular clusters. *Polym. Chem.* **2014**, *5*, 3588−3597.

(90) Sakamoto, N.; Hashimoto, T. Order-Disorder Transition of Low Molecular Weight Polystyrene-*block*-Polyisoprene. 1. SAXS Analysis of Two Characteristic Temperatures. *Macromolecules* **1995**, *28*, 6825−6834.

(91) Thelen, J. L.; Teran, A. A.; Wang, X.; Garetz, B. A.; Nakamura, I.; Wang, Z.-G.; Balsara, N. P. Phase Behavior of a Block Copolymer/Salt Mixture through the Order-to-Disorder Transition. *Macromolecules* **2014**, *47*, 2666−2673.

(92) Ruokolainen, J.; Torkkeli, M.; Serimaa, R.; Komanschek, E.; ten Brinke, G.; Ikkala, O. Order−Disorder Transition in Comblike Block Copolymers Obtained by Hydrogen Bonding between Homopolymers and End-Functionalized Oligomers: Poly(4-vinylpyridine)−Pentadecylphenol. *Macromolecules* **1997**, *30*, 2002−2007.

(93) Sun, J.; Teran, A. A.; Liao, X.; Balsara, N. P.; Zuckermann, R. N. Nanoscale Phase Separation in Sequence-Defined Peptoid Diblock Copolymers. *J. Am. Chem. Soc.* **2013**, *135*, 14119−14124.

(94) Park, S.; Lee, D. H.; Xu, J.; Kim, B.; Hong, S. W.; Jeong, U.; Xu, T.; Russell, T. P. Macroscopic 10-Terabit-per-Square- Inch Arrays from Block Copolymers with Lateral Order. *Science* **2009**, *323*, 1030−1033.

(95) Su, H.; Li, Y.; Yue, K.; Wang, Z.; Lu, P.; Feng, X.; Dong, X.-H.; Zhang, S.; Cheng, S. Z. D.; Zhang, W.-B. Macromolecular structure evolution toward giant molecules of complex structure: tandem synthesis of asymmetric giant gemini surfactants. *Polym. Chem.* **2014**, *5*, 3697−3706.

(96) Lin, Z.; Lu, P.; Yu, X.; Zhang, W.-B.; Huang, M.; Wu, K.; Guo, K.; Wesdemiotis, C.; Zhu, X.; Zhang, Z.; Yue, K.; Cheng, S. Z. D. Sequential "Click" Synthesis of "Nano-Diamond-Ring-like" Giant Surfactants Based on Functionalized Hydrophilic POSS/C60 Tethered with Cyclic Polystyrenes. *Macromolecules* **2014**, *47*, 4160−4168.